


## Article

# Effects of Metasomatism on Granite-Related Mineral Systems: A Boron-Rich Open Greisen System in the Highiş Granitoids (Apuseni Mountains, Romania)

Andrea Varga <sup>1,\*</sup> , Attila Pozsár <sup>1</sup>, Norbert Zajzon <sup>2</sup>, Boglárka Topa <sup>2</sup>, Zsolt Benkó <sup>3,4</sup>, Elemér Pál-Molnár <sup>1</sup> and Béla Raucsik <sup>1</sup>

<sup>1</sup> Department of Mineralogy, Geochemistry and Petrology, University of Szeged, H-6722 Szeged, Hungary; pozsarattila8@gmail.com (A.P.); palm@geo.u-szeged.hu (E.P.-M.); raucsik@geo.u-szeged.hu (B.R.)

<sup>2</sup> Institute of Exploration Geosciences, University of Miskolc, H-3515 Miskolc, Hungary; norbert.zajzon@uni-miskolc.hu (N.Z.); topabogi@gmail.com (B.T.)

<sup>3</sup> Isotope Climatology and Environmental Research Centre, Institute for Nuclear Research, H-4026 Debrecen, Hungary; benko.zsolt@atomki.hu

<sup>4</sup> Department of Mineralogy and Geology, University of Debrecen, H-4032 Debrecen, Hungary

\* Correspondence: raucsikvarga@geo.u-szeged.hu

**Abstract:** Greisenization is typically linked with highly fractionated granites and is often associated with hydrothermal vein systems. Late postmagmatic metasomatic processes involve the enrichment of volatile components such as boron and halogens as well as several metallic elements. The purpose of this study is to reveal the main metasomatic effects and paragenetic sequences of the related mineralizations in Highiş granitoids, Romania. In a natural outcrop, more than 30 samples were collected from granitoids, felsic veins, and country rocks. We carried out a detailed mineralogical and petrological characterization of carefully selected samples using X-ray powder diffractometry, electron microprobe analysis, and microscopic methods together with K–Ar ages of whole rocks and K-bearing minerals. Several characteristic features of albitization, sericitization, tourmalinization, epidotization, and hematitization were recognized in the studied samples. Crystallization of quartz, K-feldspar, and magnetite represents the first stage during the magmatic-hydrothermal transition. The mineral assemblage of albite, sericite, schorl, and quartz originates from the early and main stages of greisenization. While the subsequent mineral assemblages, which predominantly include dravite, specular hematite, and epidote, are closely related to the late vein-depositing stage. We propose that the study area could belong to a boron-rich open greisen system in the apical portion of Guadalupian A-type granite. Based on a new hypothesis, the previously published Permian crystallization ages (between ~272 Ma and ~259 Ma) could be homogenized and/or partially rejuvenated during the hydrothermal mineralization processes due to uraniferous vein minerals. Additionally, the Highiş granite-related system suffered a Cretaceous thermal overprint (between ~100 Ma and ~96 Ma). The results may help to understand the evolution of highly evolved granite intrusions worldwide and improve our knowledge of the effect of hydrothermal mineralization processes on the emplacement ages.

**Keywords:** greisen system; petrography; specular hematite; epidote; tourmaline chemistry; metasomatism; hydrothermal mineralization; thermal overprint



**Citation:** Varga, A.; Pozsár, A.; Zajzon, N.; Topa, B.; Benkó, Z.; Pál-Molnár, E.; Raucsik, B. Effects of Metasomatism on Granite-Related Mineral Systems: A Boron-Rich Open Greisen System in the Highiş Granitoids (Apuseni Mountains, Romania). *Minerals* **2023**, *13*, 1083. <https://doi.org/10.3390/min13081083>

Academic Editors: Chengjun Zhang, Jiaolong Zhao and Pengju He

Received: 30 June 2023

Revised: 10 August 2023

Accepted: 12 August 2023

Published: 14 August 2023



**Copyright:** © 2023 by the authors. Licensee MDPI, Basel, Switzerland. This article is an open access article distributed under the terms and conditions of the Creative Commons Attribution (CC BY) license (<https://creativecommons.org/licenses/by/4.0/>).

## 1. Introduction

Greisen systems, including highly fractionated granite batholiths (e.g., A-type granitoids) associated with hydrothermal veins, often control large-scale critical and other rare element ore deposits [1–3]. Related late to postmagmatic metasomatic processes have a close relationship with the economical enrichment of volatile components such as B, F, and Cl, and metallic elements such as Li, Be, Mo, Sn, W, Bi, U, and rare earth elements (REE). The greisen ores contain a characteristic mineral assemblage comprising quartz, muscovite,

tourmaline, topaz, and fluorite, usually adjacent to quartz–cassiterite–‘wolframite’ veins (see, e.g., [1–9]). The paragenetic sequences of greisen-related mineralizations appear to follow some general rules that could be widely applicable to most greisen deposits [1–3]. Therefore, the complex investigation of greisen systems helps us to understand the sub-solidus magmatic and magmatic-hydrothermal processes and provides us with a potential vector to discover new resources.

In the Highiş Igneous Complex (also referred to as the Highiş massive or Highiş igneous suite; [10–12]), Apuseni Mountains (Romania; Figure 1), the Middle Permian granitoid body is a classic location for the study of A-type felsic alkali rocks, including alkali feldspar granite, albite granite, and hybrid granodiorite (see, e.g., [10,11]). These post-collisional peraluminous granitoids were affected by different metasomatic and hydrothermal alterations [10–12]. Bonin and Tatu [10] highlighted that Cl-rich amphibole and coexisting F-Cl-poor to F-rich biotite are widespread throughout the Highiş felsic igneous rocks, suggesting that halogen-rich hydrothermal fluids pervasively percolated through fractures and fault zones. Furthermore, greisen veins and disseminations bearing cassiterite and rare topaz were also reported. The intrusive rocks and their associated aplitic and pegmatitic dykes as well as hydrothermal aureoles locally contain tourmaline [10,13]. However, the genetic relationship between the felsic veins and the spatially related granitoids is difficult to identify and has not been resolved by geochronology.

Within the variously deformed granitoid rocks and their contact metamorphic aureoles, the granite-related vein-type Cu-Co-Bi sulfide ore deposits were extensively studied (e.g., Şoimuş Ilii, Burdiz, and Milova Valley; Figure 2 [12,14]). These Cu-vein prospects consist of chalcopyrite, pyrite, bornite, and cobaltite, but locally pyrrhotite, pentlandite, and sphalerite also occur. The first generation of the sulfide deposits is overprinted by a secondary Au-Pb-Bi-Te-S association [12]. Quartz, apatite, siderite, and epidote are the main gangue minerals and epidote shows a REE-enrichment towards allanite-(Ce) [10,12]. Additionally, intragranitic and/or granite-related uranium mineralization also occurs in the Highiş Igneous Complex (Milova and Conop deposits), consisting of uraninite (*pitchblende*) associated with autunite and torbernite [14,15].

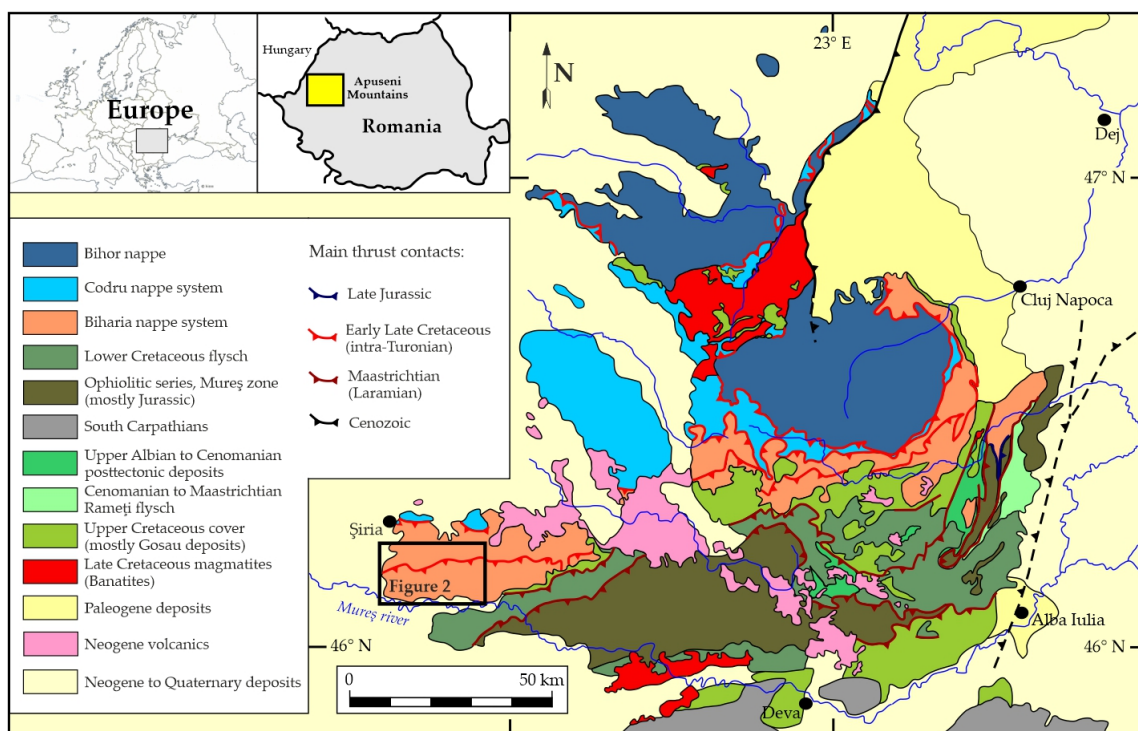


**Figure 1.** Geological and structural map of the Apuseni Mountains (modified after [16]). Top left inset shows sketch maps of the Apuseni Mountains in Romania (Europe).

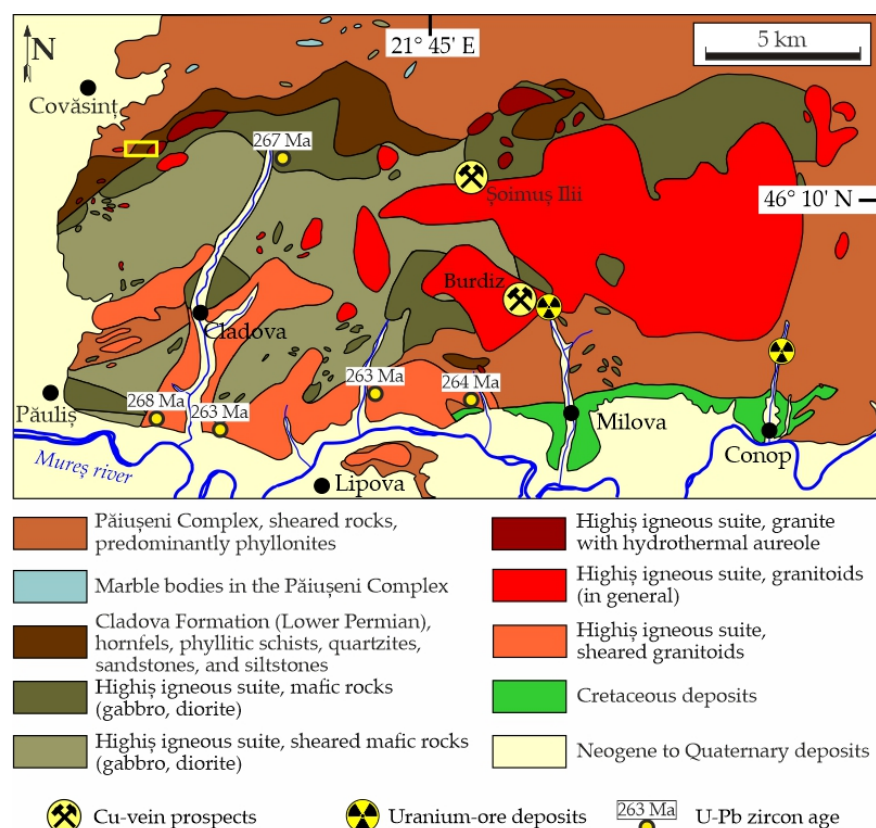


**Figure 2.** Geological map of the Highiş Igneous Complex, Apuseni Mountains (based on [17–19]), showing the study area (yellow rectangle) together with the spatial distribution of the bimodal igneous suite and the locations of important mineral deposits [12,15]. U-Pb zircon ages are from [11,20]. The legend is based on [17,19–21] and own observations.

Although several outcrops of the Highiş granitoids associated with hydrothermal veins are well-known, including tourmaline-bearing greisen veins, published mineralogical and geochronological investigations and data are relatively sparse [10–12]. The aims of this study are to describe the mineralogy and tourmaline chemistry of samples collected from a natural outcrop near Covăsinţ, corresponding to the contact aureole of the Highiş granite, and to reveal the main metasomatic effects and paragenetic sequences of related mineralizations.

## 2. Geological Background

In the Alpine–Carpathian–Dinaride orogenic system, the Apuseni Mountains are located in the southwest of Romania (Figure 1). They have been subdivided into four distinct tectonostratigraphic units, including the Bihor nappe (or autochthonous unit), Codru nappe system, Biharia nappe system (Biharia NS), and Mureş zone unit (e.g., [10,11,16–18]). The Highiş igneous suite, which is exposed in the southwestern part of the Apuseni Mountains, belongs structurally to the Biharia NS. The bimodal igneous suite is elongated in the west–east direction and comprises various rock types, including most typically mafic–intermediate intrusive rocks (gabbro, diorite, and granodiorite, respectively) and granitoids (Figure 2; see, e.g., [10,11,19–21]). The early mafic (Cladova diorite) and the late felsic (Jernova granite porphyry) intrusions have been dated by the U–Pb ID-TIMS method on zircon fractions [20], which yielded ages of  $266.7 \pm 3.8$  Ma and  $264.2 \pm 2.3$  Ma, respectively. This relatively short-lived Guadalupian (Mid-Permian) igneous event was supported by Szemerédi et al. [11] using zircon U–Pb ICP-MS data obtained from medium-grained granites (~268–263 Ma). According to Bonin and Tatu [10], a late basalt, granite porphyry, and rhyolite dyke suite crosscuts the entire plutonic complex.



The Highiş granite is typically a medium-grained equigranular granite, light in color (Figure 3), and composed of varying amounts of K-feldspar (orthoclase and microcline), quartz, plagioclase (albite), and biotite. Amphibole is minor, while zircon, apatite, monazite, allanite, Fe-Ti oxides and sulfides, fluorite, cassiterite, and rare garnet are accessory minerals [10,11]. Locally, the dominant medium-grained granites are crosscut by aplite dykes, and porphyritic microgranites also occur [11]. Based on the rock-forming mineral composition, A-type syenogranite, alkali feldspar granite, and albite granite have been distinguished. These rocks show various degrees of autometasomatism, such as albitization and hydrothermal alteration. Secondary minerals are represented by ‘sericite’/muscovite, chlorite, hematite, epidote, titanite, and tourmaline [10,11].

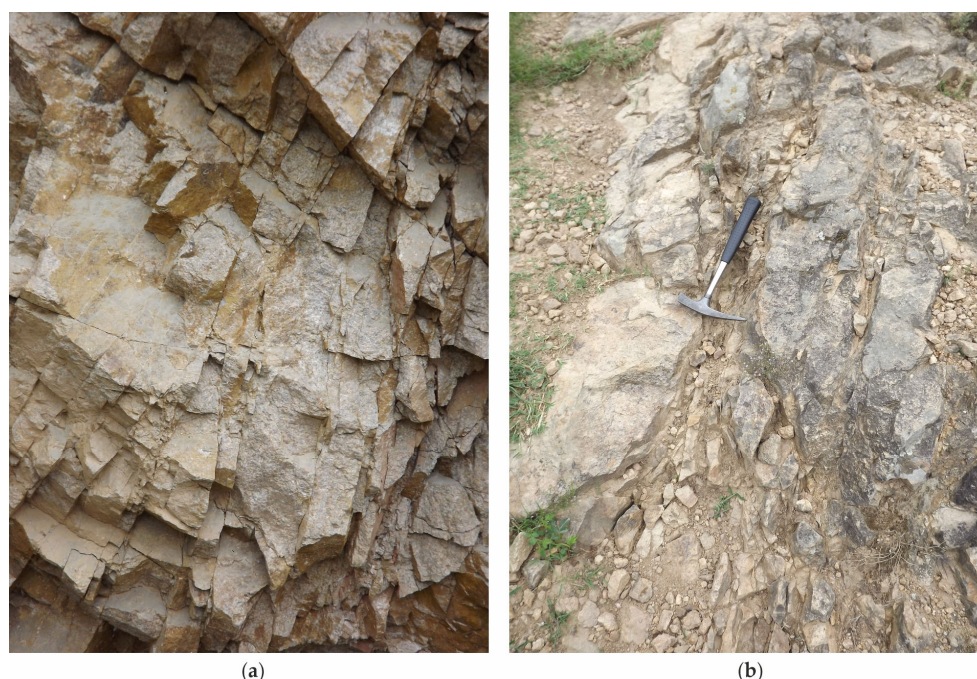


**Figure 3.** Highiş granitoids (Apuseni Mountains, Romania): (a) Outcrop of moderately tectonized medium-grained equigranular granite, Cladova valley (abandoned quarry; field of view (FOV) is about 60 cm); (b) Medium-grained granite within the faulted zone at Şoimuş hill near Lipova.

Both the igneous suite and the lower part of the Biharia NS were affected by repeated shearing events manifested in the formation of deformed rocks including phyllonites known as Paiuşeni Complex (also referred to as the Paiuşeni assemblage; see, e.g., [17,19–22]). The first shearing episode might be as old as Permian with extensive rejuvenation during the Alpine tectonism [17,22].

In the northern part of the Highiş massif, black-colored contact metamorphosed rocks occur along the boundaries of intrusive granitoid bodies (see, e.g., [12,13,19]). Hornfels associations are known as the Cladova Formation (or previously ‘Black series’), including cordierite hornfels within phyllitic schists [10,12]. These contact metamorphic rocks contain magnetite and/or ‘martite’ (pseudomorph of hematite after magnetite) associated with biotite, microcline, poikilitic tourmaline, and rare actinolite [10,13]. According to Pană and Ricman [21], the whole contact metamorphic series is interpreted as basalt hornfels. However, Bordea and Bordea [13] pointed out that, at least partially, metasediments are also present in the series. The main lithologies include massive black siltstones, gray quartzites with interbedded basic rocks, and violaceous to dark blue or black bioturbated sandstones and siltstones, representing the Lower Permian ‘Vermiculate Sandstone Formation’ known in the Bihor Mountains.

### 3. Materials and Methods

In the northwestern part of the Highiş igneous suite, near Covăşinţ (Figure 2), three locations were chosen to sample the contact aureole of the Highiş granite, representing different rock types such as granitoids, felsic veins, and country rocks (Figure 4). Sampling site KDK1 (N 46.1887562, E 21.6177805) contains phyllonites (Paiuşeni Complex) and sheared igneous rocks, sampling site KDK2 (N 46.186370, E 21.620526) comprises pelitic hornfels (Cladova Formation), and sampling site KDK3 (N 46.184206, E 21.625707) contains granitoids, felsic veins, and tourmaline-bearing hornfels. Altogether, more than 30 fresh samples were collected from every lithology of the outcrops.

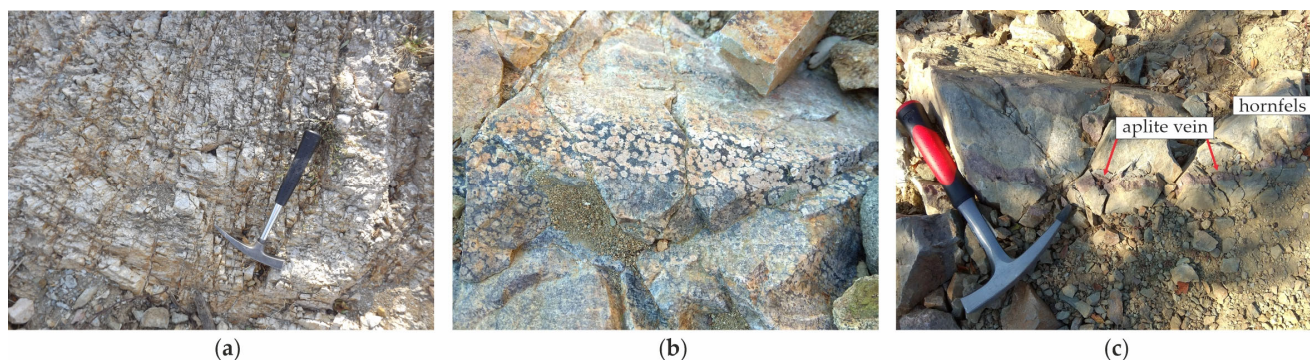


**Figure 4.** Field photographs from the natural outcrops near Covăşinţ (Apusenian Mountains, Romania): (a) Outcrop of country rocks within the shear zone at Covăşinţ (Paiuşeni Complex; sampling site KDK1); (b) Outcrop of an attractive felsic rock having a spotted or leopard appearance with light feldspar spots in a dark quartz-rich groundmass, Covăşinţ area (FOV is about 50 cm; sampling site KDK3); (c) Outcrop of hornfels (Cladova Formation; sampling site KDK3) cut by an aplite vein. In the Covăşinţ area, hornfels occurs mainly as massive, dark gray, fine-grained rock.

The whole rock's mineralogical composition and the characterization of the separated mineral fractions were measured by X-ray powder diffractometry (XRPD). A total of 12 samples (19 subsamples total) were measured at the Department of Mineralogy, Geochemistry and Petrology of the University of Szeged, Hungary. XRPD analyses were performed using a Rigaku Ultima IV X-ray diffractometer with Bragg-Brentano geometry,  $\text{CuK}\alpha$  radiation, graphite single crystal monochromator, proportional counter, divergence, and detector slits of  $2/3^\circ$ . The whole rock analysis was carried out on random powder mounts on a 'zero background' Si sample holder with the following settings: 50 kV, 40 mA, scan range from 3 to  $80^\circ 2\theta$ , goniometer step rate of  $1^\circ/\text{min}$ , data acquisition step of  $0.02^\circ$ . The clay fractions were separated by repeated ultrasonic deflocculation and gravitational settling. Oriented clay specimens were made by pipetting them onto glass slides and drying them at  $50^\circ\text{C}$ . The air-dried and ethylene-glycol solvated samples were measured using data acquisition parameters of 45 kV, 35 mA, from the scanning range of 3 to  $50^\circ 2\theta$ , goniometer step rate  $1^\circ/\text{min}$  and step width  $0.1^\circ$ . Qualitative mineralogy was determined by Match!3 software; the semiquantitative mineralogical composition was estimated using the reference intensity ratio (RIR) method.

Petrographic studies were performed on hand specimens, with the help of a hand lens and an Olympus SZX7 stereomicroscope with an Olympus UC30 digital microscope camera, and standard thin sections that were studied using an Olympus BX41 microscope under transmitted and reflected light at the Department of Mineralogy, Geochemistry and Petrology of the University of Szeged, Hungary. To determine some key minerals, a Thermo Scientific DXR Raman spectrometer was also used. Measurements were performed using an  $\times 50$  objective, 25–50- $\mu\text{m}$  pinhole aperture, and a 532-nm Nd-YAG laser with an excitation power between 0.2 and 10 mW. Cathodoluminescence (CL) microscopy of selected samples was carried out using a Reliotron VII type cold CL device mounted on an Olympus BX43 microscope (accelerating voltage: 7 kV, beam current: 0.7 mA). Photomicrographs



were made using an Olympus DP73 digital microscope camera. In this study, conventional mineral abbreviations have been used [23]. Invalid mineral names are indicated in italics.

The composition of tourmaline (sample KDK3T) was established with a JEOL JXA-8600 electron microprobe, upgraded by SAMX control, in wavelength-dispersive mode (WDX) at the Institute of Exploration Geosciences of the University of Miskolc, Hungary. An operating voltage of 20 kV and a probe current of 20 nA were used. Tourmaline samples were analyzed with the following standards: quartz (Si USNM R17701), ilmenite (Ti and Fe USMN 96189), corundum (Al USNM 657S),  $\text{MnS}_2$  (Mn synthetic), olivine (Mg USNM 111312/444), Cr-augite (Ca USNM 143965), anorthoclase (Na USNM 133868), orthoclase (K MAC 14024), and LiF (F synthetic). Fluorine was below the detection limit in the analyzed samples. PAP correction [24] was used for concentration calculations of the WDX analyses. According to Selway and Xiong [25], the chemical formulas of tourmaline were calculated on the basis of 31 O + OH + F anions, corresponding to the generalized tourmaline structural formula:  $\text{XY}_3\text{Z}_6\text{T}_6\text{O}_{18}(\text{BO}_3)_3\text{V}_3\text{W}$  [25,26], whereas the  $\text{B}_2\text{O}_3$ ,  $\text{H}_2\text{O}$ , and  $\text{Li}_2\text{O}$  content of tourmaline was calculated using stoichiometry ( $\text{B} = 3$  atoms per formula unit (apfu),  $\text{OH} + \text{F} = 4$  apfu,  $\text{Li} = 15 - \text{total} (\text{T} + \text{Z} + \text{Y})$ , respectively).

The geochronology of K–Ar isotopes was performed on four samples (vein-filling tourmaline, hornfels, and deformed country rocks), following the procedure laid out by Matsumoto and Kobayashi [27] at the Geochronology Laboratory of the Institute for Nuclear Research, Debrecen, Hungary. For mica-rich samples, whole rock and separated size fractions of phlogopite or illite were also measured. Both the  $<2\ \mu\text{m}$  and  $<1\ \mu\text{m}$  size fractions were separated from the aqueous suspension after ultrasonic disaggregation. During the K–Ar isotopic measurements, the detailed analytical processes are similar to those of Ottens et al. [28]. The accuracy and reproducibility of the isotope ratio measurements were periodically controlled with the international standards HDB-1 [29] and MDO-G [30]. The decay constants recommended by Steiger and Jäger [31] were used for the age calculation, with an overall error of  $\pm 1\%$ . The error of the samples was calculated using the equation of Quidelleur et al. [32].

## 4. Results

### 4.1. Field Observations

During field observations, various types of igneous and metamorphic rocks were identified in the study area near Covăsinț where the Highiş granite is intruded into mafic rocks and Permian siliciclastics (Figure 2). The igneous rocks are mostly granitoids, aplite, and rarely pegmatite. The metamorphic sequence comprises various types of sheared and contact metamorphic rocks (Paiuşeni Complex and Cladova Formation, respectively). Medium-grained, white to beige granites and fine-grained, pinkish aplites occur in the marginal and exterior areas of the plutonic bodies. The host rocks are greenish gray and brownish gray phyllonitic schists and metasandstones, and black and light gray, hard, massive, and banded types of hornfels; the aplite dykes and felsic veins crosscut the massive hornfels (Figure 4).

Tourmaline-bearing aplites are the most common felsic dykes (about a few centimeters thick) in the study area; however, layered aplites that consist of several bands of K-feldspar and quartz alternating with very fine-grained aplitic layers also occur (Figure 5). Pegmatites composed of quartz and K-feldspar crystals with black tourmaline were observed in the rock debris. The tourmaline crystals and aggregates show variable grain sizes and are unevenly distributed between and within samples. Many samples, such as granites, aplites, and hornfels, contain pitch black tourmaline nests and nodules (up to 7 cm in diameter). Some nodules display a leucocratic halo. The tourmaline crystals form usually massive, fine-grained aggregates but in some veins and cavities they are elongated columnar or rarely fibrous in habit. Epidote veinlets (up to about 1 cm thick) composed of epidote with variable amounts of specular hematite and goethite were observed as a late phase (Figure 5). Epidote and rare biotite also occur in cavities.

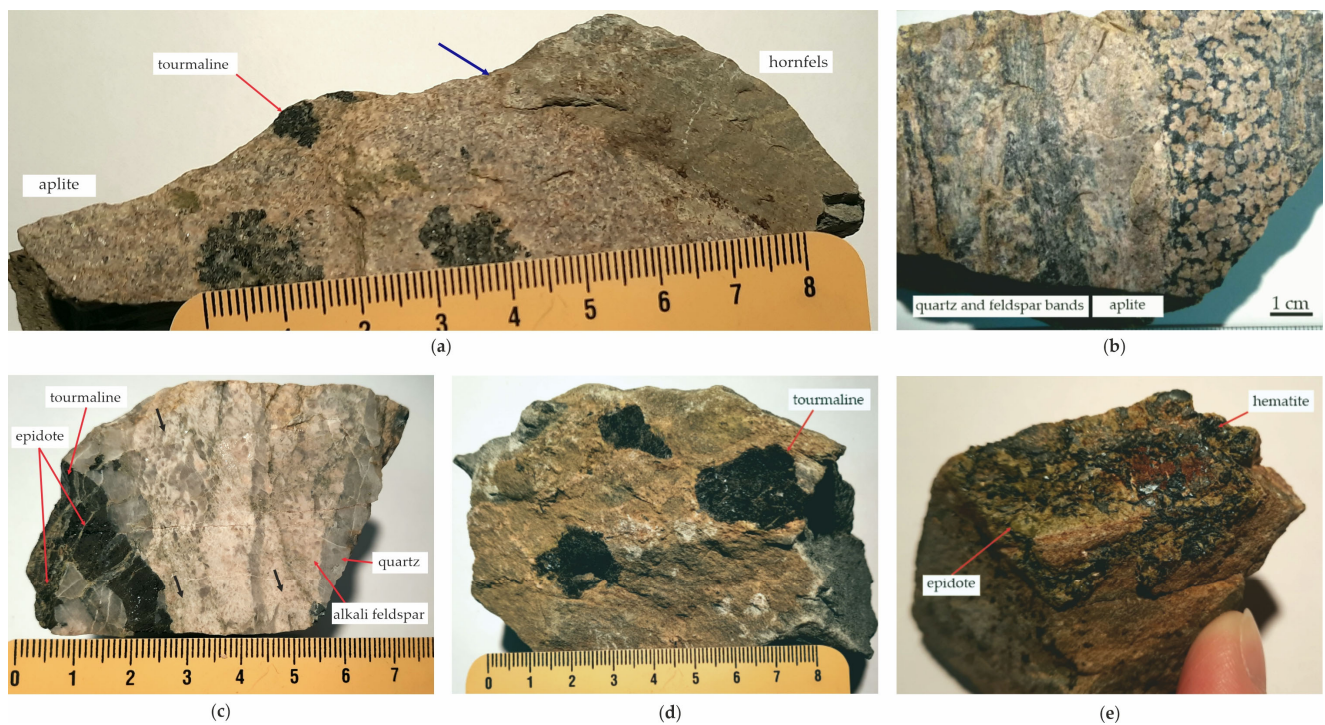


**Figure 5.** Characteristic macroscale textures of selected rocks: (a) Tourmaline nests in pinkish aplite (sample HK6). The contact between the aplite and the hornfels is highlighted by a blue arrow; (b) Layered aplite composed of very-fine-grained aplitic layers and bands of black quartz and pink feldspar (sample KDK3F); (c) Tourmaline-bearing pegmatite (sample KDK3T) consisting of an intimate intergrowth of alkali feldspar and quartz (black arrows); (d) Tourmaline nests in hornfels (sample HK8); (e) Epidote and partially goethitized ‘specularite’ (a variety of hematite) vein fillings in hornfels (sample HK18; FOV is about 6 cm).

#### 4.2. XRPD Analyses

Based on semiquantitative XRPD analysis, each studied rock type can be characterized by a very different mineralogical composition (Table 1).

**Table 1.** Semiquantitative mineralogical composition of selected samples.

Sampling Site/Type	Sample Code/Type	Minerals (~wt%)
KDK3 (granitoids)	HK2 granite (WR) <sup>1</sup>	Pl (40), Kfs (38), Qz (20), Cal (2)
	HK2 tourmaline, nest	Qz (51), Tur (49)
KDK3 (dykes/veins)	KDK3F (VM) <sup>2</sup>	Qz (63), Kfs (21), Pl (16)
	KDK3T (VM)	Pl (68), Qz (32)
	KDK3T tourmaline	Qz (44), Tur (37), Ep (19)
	HK17 (WR excluding tourmaline)	Pl (82), Amp (12), Ms (6)
	HK18 (VM)	Hem (57), Ep (43)
	HK18 specularite	Ep (53), Hem (47)
KDK3 (hornfels)	HK19 specularite	Hem (91), Bt (9)
	HK8 (WR)	Pl (76), Bt (22), Hem (2)
	HK11 (WR)	Pl (65), Bt (21), Ms (14)
	HK11 light spots	Pl (51), Bt (46), Hem (3)
KDK2 (hornfels)	HK11 mica-rich part	Pl (47), Hem (19), Qz (19), Bt (15)
	KDK2B (WR)	Ms (47), Qz (30), Chl (17), Hem (6)
	KFS3 (WR)	Pl (63), Crd (15), Qz (12), Bt (5), Hem (5)

Table 1. Cont.

Sampling Site/Type	Sample Code/Type	Minerals (~wt%)
KDK1 (country rocks)	KDK1L (WR)	Ms (52), Qz (22), Pl (20), Chl (6)
	KDK1L clay fraction	Illt ± Ms (65), Vrm ± Chl/Vrm (24), Kln (11)
	KDK1S (WR)	Qz (33), Pl (30), Ms (22), Chl (15)
	KDK1S clay fraction	Illt ± Ms (49), Vrm ± Chl/Vrm (25), Chl (13), Kln (13)

<sup>1</sup> WR: whole rock, <sup>2</sup> VM: vein minerals. Mineral abbreviations: Amp, amphibole; Bt, biotite; Cal, calcite; Chl, chlorite; Crd, cordierite; Ep, epidote; Hem, hematite; Illt, illite; Kfs, K-feldspar; Kln, kaolinite; Ms, muscovite; Pl, plagioclase; Qz, quartz; Tur, tourmaline; Vrm, vermiculite.

Felsic rock samples represented by granite and quartz-feldspar veins are predominated by quartz (~20–68 wt%), probably albitic plagioclase (~16–82 wt%), and K-feldspar (~21–38 wt%), locally, with minor amphibole (~12 wt%), white mica (~6 wt%), and calcite (~2 wt%). The tourmaline concentrates are composed of tourmaline, quartz, and epidote. Separated fragments of well-crystallized specular hematite with a platy appearance contain hematite, epidote, and minor biotite (Appendix A, Figure A1).

The whole rock samples of hornfels do not show a uniform mineralogical composition, the only common property being that they are usually rich in albitic plagioclase (up to 76 wt%) and biotite (up to 22 wt%). Massive hornfels samples are composed of albitic plagioclase, biotite (in samples HK8 and HK11, probably close to the phlogopite endmember), white mica, hematite, and quartz. In pelitic hornfels, locally showing relic sedimentary lamination, albitic plagioclase, white mica, quartz, chlorite, cordierite, hematite, and biotite are the detected minerals (Appendix A, Figure A1).

The mica-rich, foliated country rocks are composed of abundant white mica, quartz, and plagioclase with a subordinate amount of chlorite. Their separated clay fraction (<2 µm) exhibits an illite-rich composition (~49 and ~65 wt%) with vermiculite (±mixed-layer chlorite/vermiculite), chlorite, and minor kaolinite (Table 1).

#### 4.3. Petrography

The mineral compositions of the granitoid rocks and felsic veins are essentially the same in the study area, so they are described together (Figure 6). Granite and aplitic rocks are composed of K-feldspar (orthoclase and microcline), sodic plagioclase, quartz, and rare biotite and muscovite. Tourmaline, apatite, zircon, and opaque minerals are the typical accessories. The anhedral to subhedral granular texture and perthite are its dominant characteristics. Sericite is a secondary replacement that is developed locally in the feldspars; additionally, secondary chlorite partially replaces biotite. In layered aplite, quartz and K-feldspar bands are rich in disseminated opaque minerals with square, trapezoid, and triangular sections; furthermore, quartz crystals have tiny opaque inclusion-rich cores. Raman measurements indicate that these crystals are most likely secondary hematites, but the presence of primary magnetite can be assumed (characteristic bands: ~225, ~290, ~410, and ~660 cm<sup>-1</sup>; <http://rruff.info/>, accessed on 21 May 2023 [33]), which is also supported by the cubic shape. Graphic and micrographic textures are the most important characteristics of pegmatite, containing large crystals of quartz, alkali feldspar, and tourmaline. In these felsic rocks, albitization of the primary K-feldspars is a common feature. Epidote and rare secondary biotite and muscovite occur as disseminated crystals or veinlets.

The felsic rock samples contain at least two generations of tourmaline (groups I and II), indicating that these rocks were affected by multiple hydrothermal events (Figure 7). Group I tourmaline occurs as disseminated crystals, crystal aggregates, or veinlets. It is ocher or brown with strong pleochroism from brown to pale and is generally homogenous, anhedral, and poikilitic, mainly containing quartz and feldspar mineral inclusions. In some cases, group I tourmaline shows dark and light brown optical zoning or mottled color. In a single sample, titanite occurs as inclusion in a poikilitic tourmaline that coexists with amphibole and plagioclase. Group II tourmaline typically overgrows group I tourmaline



and occurs as replacement, crack fillings, or as euhedral crystals associated with quartz. This later generation of tourmaline is generally blue to grayish blue and displays weak pleochroism from pale to dark blue, and often shows irregular optical zoning. Group II tourmaline crystals are subhedral to euhedral. They typically coexist with epidote, biotite, and partially goethitized hematite grains supported by Raman measurements (characteristic bands:  $\sim 225$ ,  $\sim 244$ ,  $\sim 290$ ,  $\sim 300$ ,  $\sim 385$ ,  $\sim 410$ , and  $\sim 480$   $\text{cm}^{-1}$ ; <http://rruff.info/>, accessed on 21 May 2023 [33]). Rarely, K-feldspar also occurs as microcrack fillings in tourmaline.

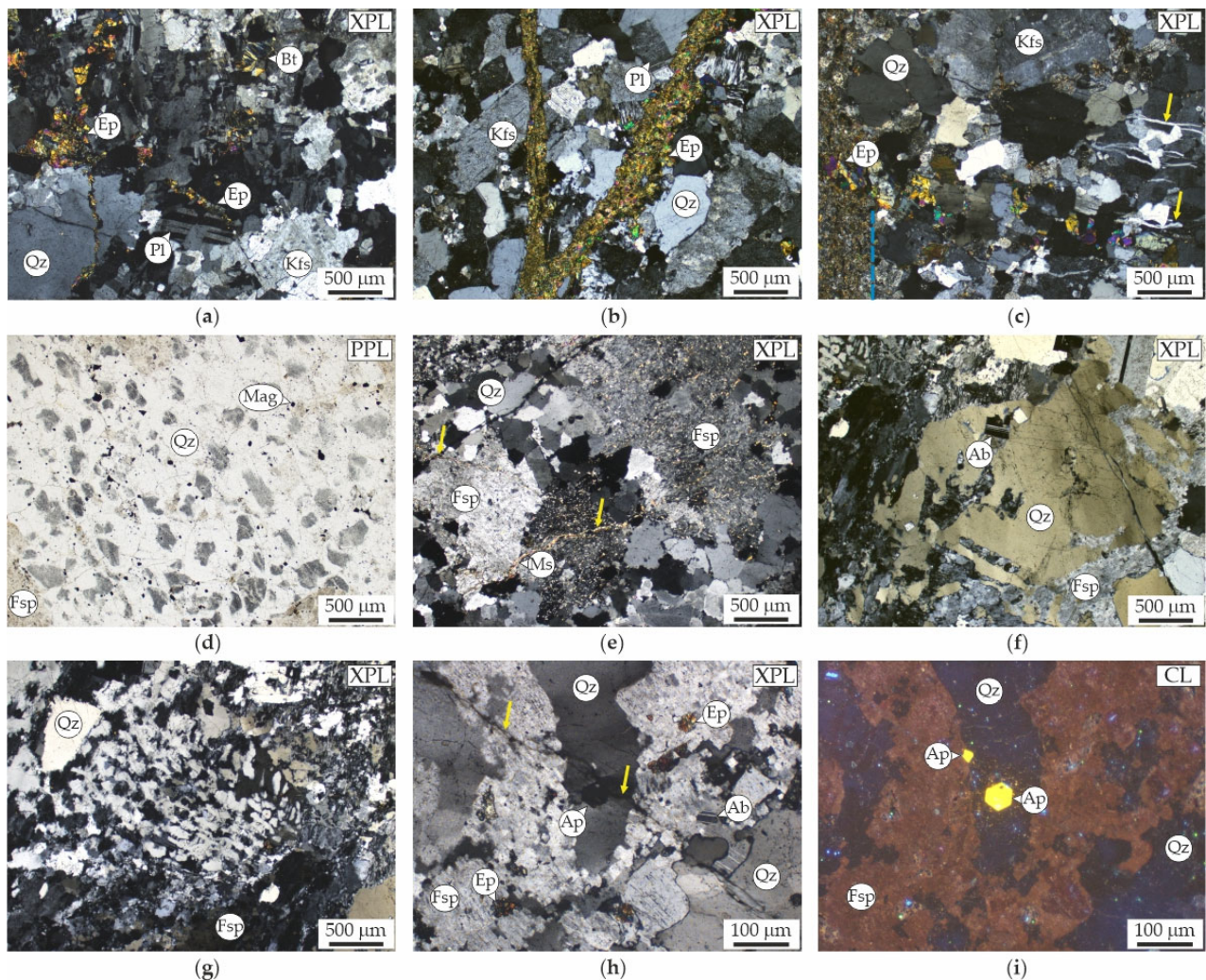


**Figure 6.** Photomicrographs of selected granitoid rocks: (a) Hydrothermally altered granite (sample HK2). The epidote occurs as disseminated crystals and veinlets; (b) Epidote veinlets in aplite (sample HK12); (c) Thin quartz (yellow arrows) and epidote veinlets in aplite (sample HK6). The contact between the aplite and the hornfels is highlighted by a blue dashed line; (d) Opaque inclusion-rich quartz grains in a quartz and feldspar band (sample KDK3F); (e) Sericitized K-feldspars in layered aplite (sample KDK3F) with very thin monomineralic white mica (muscovite) veinlets (yellow arrows); (f,g) Micrographic texture in pegmatite (sample KDK3T). Alkali feldspars show a mottled, blocky to tabular sector extinction pattern, suggesting extensive albitization; (h,i) Albitized feldspars show a dull brown CL color. Near microcracks (yellow arrows), small apatite grains show bright yellow luminescence (sample KDK3T). Mineral abbreviations: Ab, albite; Ap, apatite; Bt, biotite; Ep, epidote; Fsp, feldspar; Kfs, K-feldspar; Mag, magnetite; Ms, muscovite; Pl, plagioclase; Qz, quartz. Other abbreviations: CL, cathodoluminescence; PPL, plane-polarized light; XPL, cross-polarized light.



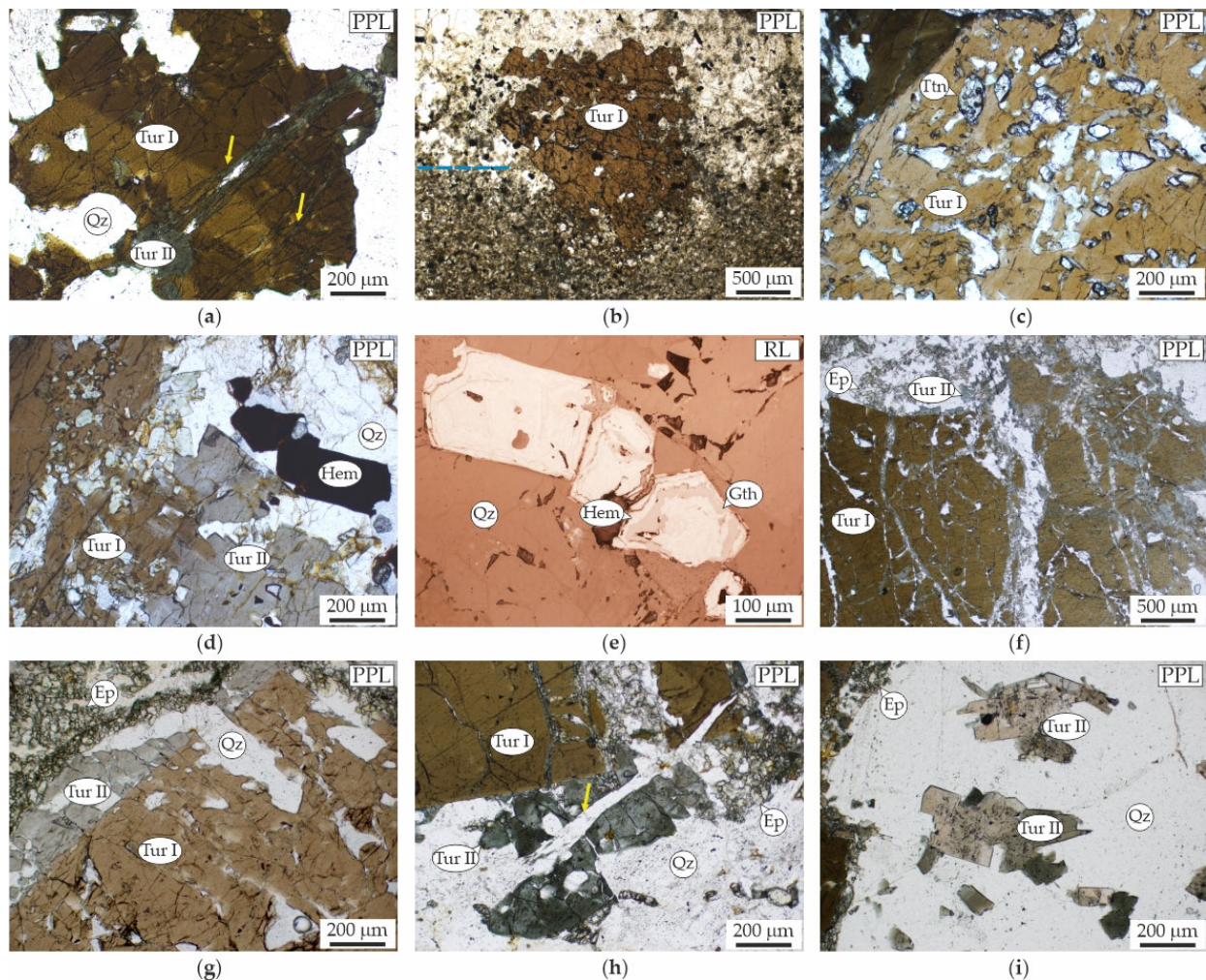


**Figure 7.** Photomicrographs of tourmaline textures: (a) Optical zoning of group I tourmaline in granite (sample HK2). The anhedral and poikilitic tourmaline is yellowish brown and crosscut by microcracks (yellow arrows) along with group II tourmaline; (b) Brown anhedral tourmaline in aplite (sample HK6). The contact between the aplite and the hornfels is highlighted by a blue dashed line; (c) Poikilitic tourmaline with titanite mineral inclusions (sample HK17); (d,e) Partial alteration of the group I tourmaline (hereafter referred to as transition between groups I and II tourmalines): group II tourmaline often replaces the earlier generation of tourmaline, producing a mottled appearance. The later generation of tourmaline coexists with partially goethitized hematite (sample HK17); (f–i) Group II tourmaline overgrows group I tourmaline and occurs as crack fillings, rims, or as tiny euhedral crystals (sample KDK3T). Mineral abbreviations: Ep, epidote; Gth, goethite; Hem, hematite; Ttn, titanite; Tur, tourmaline; Qz, quartz. Other abbreviations: PPL, plane-polarized light; RL, reflected light.

In the contact metamorphic aureole, various types of hornfels such as albite-biotite hornfels, and cordierite hornfels occur (Figure 8). Albite-biotite hornfels is fine-grained and massive with a granoblastic texture. It consists of albite and biotite as major minerals. Additionally, porphyroblastic biotite can form dark clots. Disseminated opaque grains, most likely hematite (Table 1), are also common and locally limonitized. Tourmaline occurs in nests (group I; Figure 5b) or forms dark clots (group II) that show a close relationship with plagioclase, quartz, biotite, epidote, and hematite. Cordierite hornfels is a dark gray to black rock, locally showing foliation and primary bedding. Its main minerals are plagioclase, cordierite, quartz, and mica (biotite and muscovite). This rock shows a spotted porphyroblastic texture with cordierite porphyroblasts. Moderately to strongly foliated



phyllonites consist of muscovite bands, granoblastic quartz, plagioclase, chlorite, apatite, and opaque minerals (Figure 8).

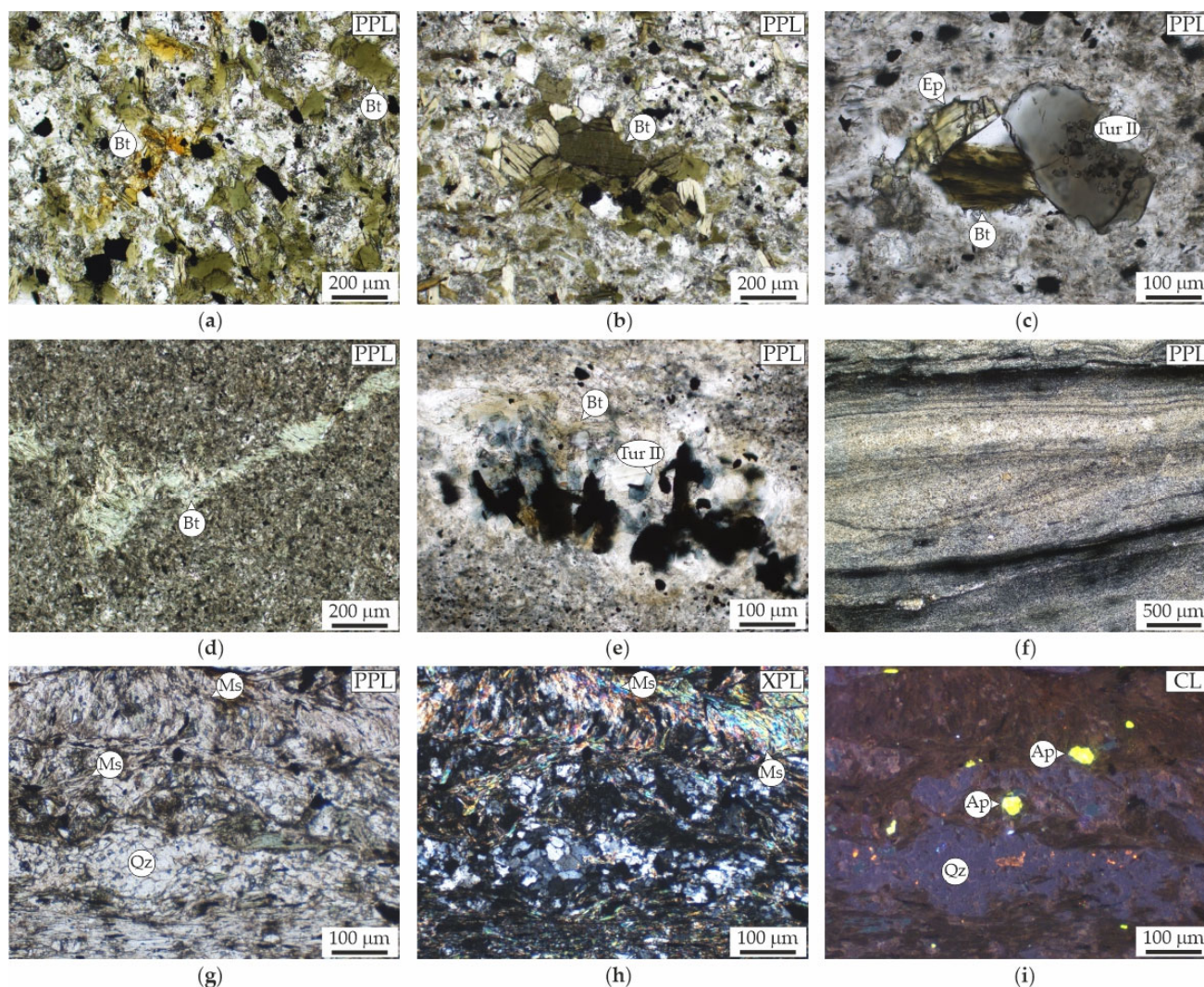


**Figure 8.** Photomicrographs of country rocks: (a) Biotite-rich hornfels (sample HK8); (b) Biotite aggregate with feldspar and opaque grains in massive hornfels (HK8); (c) Inclusion-rich grayish blue tourmaline with epidote and biotite in massive hornfels (HK11); (d) Fine-grained hornfels with a biotite veinlet (KDK2B); (e) Quartz-tourmaline clot with biotite and opaque grains in pelitic hornfels (KFS1); (f) Relic sedimentary microstructures in cordierite hornfels (KFS3); (g–i) Quartz, muscovite, and apatite in phyllonite (KDK1). Mineral abbreviations: Ap, apatite; Bt, biotite; Ep, epidote; Ms, muscovite; Tur, tourmaline; Qz, quartz. Other abbreviations: CL, cathodoluminescence; PPL, plane-polarized light; XPL, cross-polarized light.

#### 4.4. Mineral Chemistry of Tourmaline

Vein tourmaline samples have been subjected to crystal-chemical investigation, containing the most common tourmaline group I (dark/light ocher and brown) overgrown by rims of group II (dark/light blue) tourmaline. Their chemical compositions fit the schorl–dravite solid solution.

Representative chemical analyses of tourmaline group I are given in Appendix B, Table A1. Based on the major and minor elements composition, two populations of group I tourmaline can be distinguished. At the X-site, alkali metals dominate since the Na content varies mostly between 0.56 and 0.69 apfu (type 1 tourmaline). Thus, this tourmaline belongs to the alkali group; however, the amount of Ca is also significant (up to 0.38 apfu).



Some samples, corresponding to the type 2 tourmaline, have an elevated Ca component (up to 0.53 apfu) and calcic character. Group I tourmaline shows a higher value than the ideal 6.00 apfu Si in the T-site, suggesting that some ferric iron should be present in the Z- and/or Y-positions. At the Y-site, the ferrous iron is dominant (1.72–2.34 apfu). Type 1 tourmaline has a relatively high amount of Mg (up to 1.31 apfu) whereas type 2 tourmaline has a relatively high amount of Ti (up to 0.16 apfu), Mn (up to 0.02 apfu), and  $\text{Fe}^{2+}$  (up to 2.34 apfu) in this crystallographic position. Based on its crystal-chemistry, tourmaline group I represents the schorl mineral species.

Representative chemical analyses of tourmaline group II are given in Appendix B, Table A2. Group II tourmaline is compositionally slightly variable. At the X-site, alkali metals predominate since the Na content varies between 0.68 and 0.80 apfu; the amount of Ca is not significant (between 0.06 and 0.24 apfu). Relatively Ca-rich compositions occur in the transition from group I to group II tourmaline. Thus, group II tourmaline also belongs to the alkali group. They show 5.98 to 6.04 apfu Si in the T-site, while the Z-site is almost fully occupied by Al. The Y-site shows the common mixed cation occupancy. In this position, the Mg content is dominant (1.43–1.96 apfu) and the ferrous iron content is also significant (0.85–1.55 apfu), while the amount of Al, Ti, and Mn is negligible (0–0.14 apfu, 0.01–0.06 apfu, and 0–0.01 apfu, respectively). In the transition from group I to group II, the tourmaline is poorer in Mg and slightly richer in ferrous iron and Ti than the typical group II tourmaline (type 3). Based on its crystal-chemistry, tourmaline group II represents the dravite mineral species.

#### 4.5. K–Ar Geochronology

Geochronological investigations were performed on granite-related vein tourmaline, hornfels, and deformed country rocks (phyllonites), to obtain some time constraints on the formation of contact metamorphism and secondary mineralization during shearing. Four samples were selected for examination. The analytical results are presented in Table 2. The K–Ar ages are between  $133.61 \pm 1.90$  Ma and  $75.55 \pm 1.08$  Ma. Interestingly, both the tourmaline-rich sample with K-feldspar crack fillings and hornfels yielded Cretaceous ages. The bulk phyllonite samples yielded an age of  $112.16 \pm 1.60$  Ma and  $126.37 \pm 1.98$  Ma, respectively (Early Cretaceous). Their illite concentrates contained 6.28 and 3.21 wt% K in the  $<2 \mu\text{m}$  fraction. The determined K–Ar ages are  $95.66 \pm 1.37$  Ma and  $97.68 \pm 1.40$  Ma. In the  $<1 \mu\text{m}$  fraction, the illite yielded an age of  $75.55 \pm 1.08$  Ma. Obviously, the K–Ar age decreases with decreasing grain size, indicating an increase in the authigenic/detrital ratio with decreasing grain size. An interpretation of the age data is given in the discussion.

**Table 2.** Results of the K–Ar analysis of the whole rocks and separated fractions.

Sample Type	Mineral	$r$ $^{40}\text{Ar}^*/^{40}\text{Ar}_{\text{tot}}$	$^{40}\text{Ar}^*/\text{m}$ $\times 10^{-6}$ [ccSTP/g]	K (wt%)	Age (Ma)
tourmaline HK17	tourmaline + K-feldspar	0.37	1.60	0.4	$100.26 \pm 1.44$
hornfels HK8 (WR) <sup>1</sup>	biotite (phlogopite)	0.68	1.49	3.035	$133.61 \pm 1.90$
$<2 \mu\text{m}$ fraction		0.66	16.62	3.951	$105.14 \pm 1.50$
$<1 \mu\text{m}$ fraction		0.41	15.08	3.813	$98.96 \pm 1.42$
KDK1L (WR)	illite	0.63	19.19	4.267	$112.16 \pm 1.60$
$<2 \mu\text{m}$ fraction		0.50	23.96	6.275	$95.66 \pm 1.37$
KDK1S (WR)	illite	0.15	2.70	0.53	$126.37 \pm 1.98$
$<2 \mu\text{m}$ fraction		0.40	12.50	3.205	$97.68 \pm 1.40$
$<1 \mu\text{m}$ fraction		0.58	1.15	3.833	$75.55 \pm 1.08$

<sup>1</sup> WR: whole rock.

## 5. Discussion

### 5.1. Main Metasomatic Effects and Paragenetic Sequence

In the study area, granitic pegmatites and aplites represent the final stage of magmatic crystallization. The primary rock-forming minerals are abundant quartz, alkali feldspar, plagioclase, and rare biotite, corresponding to the initial mineral assemblage (Figure 6a,f,g). In the layered aplite, quartz and feldspar bands form an attractive and specific textural feature that can be interpreted as unidirectional solidification texture (UST; [34]). Clots or thin layers of pink K-feldspar crystals form USTs within nearly parallel to highly contorted layers of black quartz. UST quartz is intensely impregnated with Fe-oxides (Figure 6d); most likely, the primary oxide phase was magnetite that was partially oxidized to hematite during subsequent processes. According to Müller et al. [34], magnetite can be co-genetic with UST quartz, forming combined layers. Furthermore, quartz UST crystallization represents the first stage during the magmatic-hydrothermal transition associated with overpressured volatiles and fluids between 770 °C and 590 °C [2,34].

Based on our petrographic results (Figures 6e,f and 7a–c, Table 1), the primary mineral assemblage was first overprinted by albitization and sericitization associated with tourmalinization (group I tourmaline: schorl with quartz). Furthermore, Bonin and Tatu [10] published evidence that the Highiş granite suffered alkali metasomatism (microclinization and albitization). These authors observed quartz-mica-microcline-albite-tourmaline-cassiterite-topaz-bearing disseminations, veins, and pipes in the southern part of the Highiş igneous suite. The calculated temperature interval of metasomatism by halogen-bearing aqueous fluids could be between 640 °C and 410 °C using Ti-in-biotite geothermometer [10]. In general, an early alkaline stage was proved during greisenization processes (Figure 9; see, e.g., [1–3,35]), resulting in the destabilization and related destruction of primary feldspars and biotite. Subsequently, corresponding to the greisenization stage, white mica (muscovite and/or phengite) forms as replacement or monomineralic selvages along fractures. In addition, Fe-rich tourmalines, such as schorl, are typically found in ore deposits of greisen affinity [2,3,36]. Although characteristic mineral associations, including fluorite, topaz, and Sn-W-ore minerals, do not occur in the study area near Covăsinţ, we propose that the mineral assemblage of albite, sericite (white mica), schorl, and quartz-originate from the early and main stages of greisenization (Figure 9).

The next stage is characterized by tourmalinization (group II tourmaline: dravite with quartz), epidotization, and hematitization together with the subsequent formation of albite and micas (dravite + quartz + specular hematite + epidote + apatite → albite + muscovite and/or biotite/phlogopite). As a second-generation boron mineral, Mg-rich tourmaline, such as Mg-rich schorl and dravite, was documented during greisen alteration, representing a younger postmagmatic phase [2,3,36]. In the studied samples, ‘*specularite*’ can be used as a key temperature indicator within this stage because this morphological type of hematite tends to form associated with fluids between ~360 °C and ~200 °C (see, e.g., [37]). Therefore, this paragenesis could indicate a metasomatic environment with decreasing temperature and increasing alkalinity (Figure 9).

It is important to note that epidote-apatite-quartz-siderite veins with disseminated Cu-mineralization (mainly chalcopyrite and bornite) have previously been documented in the vicinity of the contact between granite and mafic hornfels [10,12]. According to Ciobanu et al. [12], this mineralization was related to the mafic suite or associated with the granite. On the one hand, however, the paragenetic sequences of greisen systems follow some general rules [1–3,5]. Deposition of the ore minerals typically starts with an Sn-W oxide phase, followed by common sulfides (e.g., porphyry Cu-Au-Mo-ore deposits), and then a late oxide phase characterized by Fe-oxides associated with carbonates [1–9,36]. On the other hand, tourmalinization, epidotization, and hematitization are also observed in the contact metamorphic aureole in the study area (Figure 8); therefore, we suggest that this mineral assemblage, including epidote and apatite, is closely related to the late vein-depositing stage of the greisenization processes (Figure 9). During greisenization, epidote precipitation can trap much of the light REE [8], which is consistent with the

observation that the epidote in the Highış massive was enriched in the light REE toward allanite-(Ce) [12].

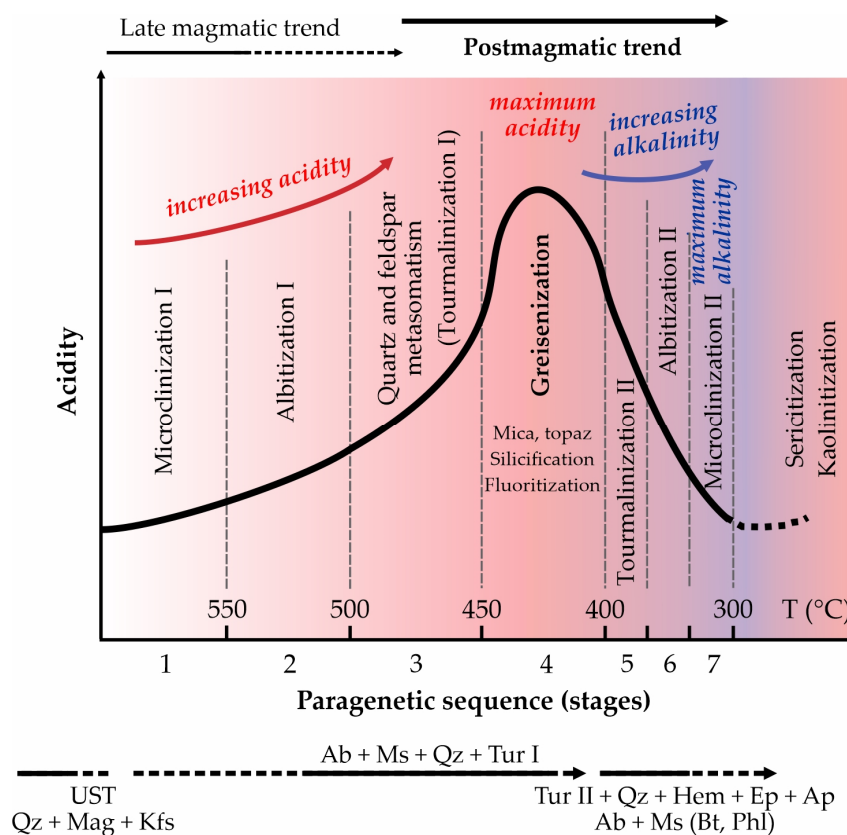


**Figure 9.** Schematic illustration of the late to postmagmatic trends of greisen deposits in granite, corresponding to the evolution of acidity and temperature over time [1–3,35]. The most important metasomatic mineral assemblages in the study area are also shown at the bottom of the figure. Mineral abbreviations: Ab, albite; Ap, apatite; Bt, biotite; Ep, epidote; Hem, hematite; Kfs, K-feldspar; Mag, magnetite; Ms, muscovite; Phl, phlogopite; Tur, tourmaline; Qz, quartz. Other abbreviations: UST, Unidirectional solidification texture.

### 5.2. Tentative Reconstruction of the Greisen System in the Study Area

Greisenization, corresponding to a granite-related postmagmatic alteration process, typically takes place in the apical portions of intrusive bodies (Figure 10). In the study area, the aplitic and pegmatitic rock domains occur together with the UST quartz and K-feldspar layers, which are direct field evidence for the cupola zones, reflecting a district-scale vector for granite-related ore deposits, depending on the levels of uplift and/or erosion [34]. Abundant tourmaline that forms clots or nests in the granitoid rocks (Figures 5a,c and 7) reflects a boron-rich greisen system which is usually not ore mineralized [2,3]. These characteristics are indicative of an endogreisen system within the intrusion (Figure 10), in which albitization also played an important role (see, e.g., [1–3,35,36]).

The country rocks also contain disseminated tourmaline (Figures 5d and 8c,e); additionally, the tourmaline-quartz-dominated assemblages form crosscutting veins, suggesting an open system during the greisen alteration processes. This structural relationship attests to an exogreisen system in which boron-bearing fluids can easily escape along fractures to different country rocks and are channeled along joints and faults, forming pervasive tourmalinization and vein systems [2,3,36]. During the mixing of magmatic and meteoric waters, postmagmatic volatiles can circulate between granitoids and host rocks [36]. According to Pirajno [2,3], in pelitic and psammitic rocks, a narrow contact metamorph aureole could form, including spotted schists with the presence of porphyroblastic biotite and cordierite. Greisenization often overprints thermal mineral assemblages and is typi-



cally characterized by the nucleation of muscovite, albite, and tourmaline. In mafic country rocks, the greisen alteration can be associated with the presence of quartz, plagioclase, muscovite, phlogopite, actinolite, and chlorite. The observed mineralogical composition together with the petrographic features (Figure 8, Table 1) shows that the exogreisen deposits were developed in both aluminosilicate and mafic rocks in the study area (Figure 10; pelitic and mafic hornfels, respectively).

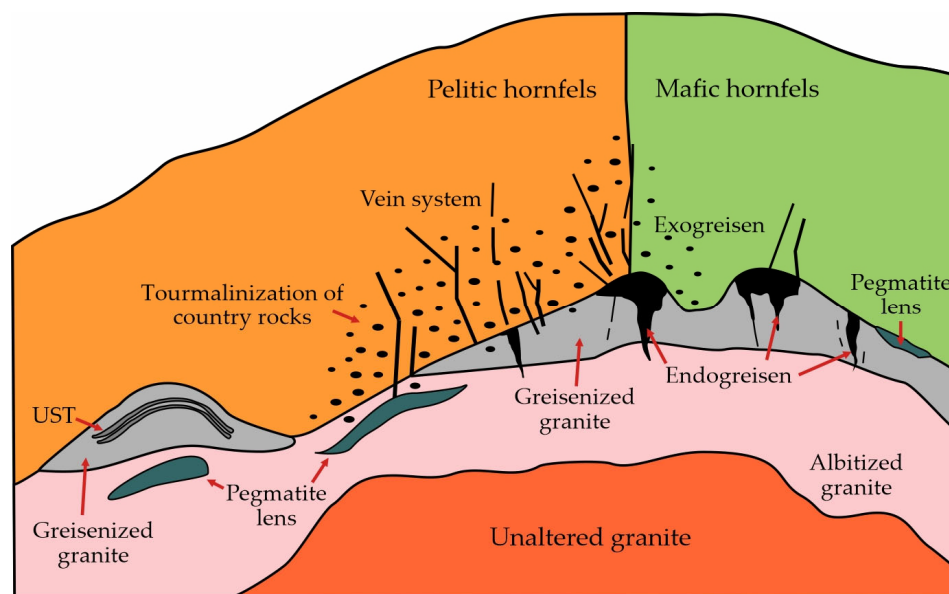


**Figure 10.** Schematic diagram showing distribution of various textures, corresponding to the endo- and exogreisen systems, in the apical zone of a greisenized intrusion [1–3,34–36]. Abbreviations: UST, Unidirectional solidification texture. The study area corresponds to a boron-rich open greisen system. Its exogreisen deposits were developed in both aluminosilicate and mafic rocks.

### 5.3. Interpretation of the Age Data

Previous ID-TIMS U–Pb zircon geochronology suggests a Middle Permian (Guadalupian) age for the Highış Igneous Complex. The ages gained from three multigrain fractions of colorless and euhedral zircon are  $266.7 \pm 3.8$  Ma and  $264.2 \pm 2.3$  Ma for early mafic and late felsic suites, respectively, bracketing the age of magmatism [20]. The reported emplacement ages were verified by recent ICP-MS U–Pb zircon geochronology of the Highış granite ( $267.8 \pm 4.4$  Ma,  $263.2 \pm 4.4$  Ma, and  $262.9 \pm 4.1$  Ma; [11]). Based on these data, the emplacement of the mafic pluton is between 271 Ma (the oldest crystallization age) and 263 Ma (the youngest crystallization age) whereas that of the granite intrusion is between 272 Ma and 259 Ma. The crystallization ages overlap each other in an obvious window between 271 Ma and 263 Ma, and the data suggest that the felsic suite could be even older; however, field relationships clearly indicated that an early mafic phase was followed by granitic intrusion and veining [10,19–22]. Regarding spatial distribution, the oldest granite is relatively far away from the known Cu-vein prospects and U-deposits (Figure 2). This suggests that the crystallization ages could be homogenized and/or partially rejuvenated during the hydrothermal mineralization processes.

According to Bonin and Tatu [10], the entire igneous complex was pervasively permeated by halogen-rich hydrothermal fluids. The supposed hydrothermal episodes would have occurred during a ~150 My-long period of time, extending from the Guadalupian to the Middle Cretaceous. Obviously, granite-related postmagmatic hydrothermal activities that occur during this broad time span are highly unlikely. However, mineralization that occurs millions of years after the emplacement of a pluton may become a reality. Mohammadi et al. [5] and Liu et al. [38] pointed out that there is another source of heat that can be involved in the postmagmatic hydrothermal activity associated with greisenization. The

formation of uraniferous greisen veins can be associated with the high heat-producing (HHP) nature of a pluton, resulting from radioactive decay. For example, based on the U–Pb geochronology of hydrothermal monazite, the time gap between the emplacement of the granite pluton (Mount Douglas Granite, New Brunswick, Canada) and the time of the youngest mineralization can be longer than 20 My [5]. The results of the finite element numerical modeling of Liu et al. [38] indicate that an increase of 500 to 1000 m in magma thickness can prolong the suprasolidus lifetimes of HHP magmas by 50 to 74%.

Unfortunately, there are no data to demonstrate any relationships between the emplacement timing of the Highiş granite and postmagmatic activities in this magmatic–hydrothermal system. New K–Ar geochronological investigations on the vein tourmaline (K-bearing phase: K-feldspar crack fillings) and massive hornfels (phlogopite) yielded Cretaceous ages (Table 2), reflecting a late thermal overprint discussed below. However, the uraniferous nature of the Highiş granite has been previously reported by Ciobanu et al. [12] and Bejenaru and Cioloboc [14], and the references therein. Complex hydrothermal parageneses, including base metals (e.g., cobaltite, chalcopyrite, galena, galenobismutite, and native bismuth), with locally U-, Th-, and REE-bearing minerals were described in the extensively explored vein prospects such as Şoimuş Ilii and Burdiz (Figure 2). Uraniferous veins, containing U-, Th-, and REE-bearing minerals (e.g., ‘pitchblende’, monazite, zircon, apatite, and REE-carbonates), have been reported mainly from the southern part of the igneous complex [12,14].

As a working hypothesis, we propose that metals become concentrated in late-stage melts and exsolving hydrothermal fluids related to the Highiş granite intrusion. These fluids could migrate within the pluton and generate ore lenses and mineralized greisen veins, as well as greisenized zones in the country rocks. Therefore, the aforementioned U–Pb zircon ages, especially the younger ones, could date postmagmatic hydrothermal mineralizations instead of the crystallization ages of the Highiş granite intrusion, which could be substantially older within a few million years. Future geochronological work on the Highiş granite and country rock samples will provide an important test of this hypothesis. However, the results of our case study highlight the fact that fluid-controlled processes related to greisenization can influence even geochronological data obtained from granitoid rocks. Consequently, in geologically analogous cases, these possible effects must also be considered when interpreting radiometric age data.

In the Highiş Mountains, previously published conventional K–Ar ages, which are useful for defining cooling histories, range between 123 Ma and 113 Ma for phyllonites (Căsoaia and Şiria), suggesting the effect of Cretaceous tectonism and concomitant low-grade metamorphism at temperatures decreasing from ~400 °C to ~250 °C (see, e.g., [10,12,17] and references therein). Additionally, whole rock phyllonite samples within the shear zone yielded an  $^{40}\text{Ar}/^{39}\text{Ar}$  plateau age of 114 Ma for the Cladova Formation (‘Black series’ near Cuvin) and an age of 100 Ma for the Paiuşeni Complex (near Covăsinţ), closely dating development of the mylonitic fabric via synkinematic growth of white mica [17].

The Cretaceous (mainly Albian–Aptian) thermal episodes are verified by our K–Ar data (Table 2). Regarding the closure temperature of the K–Ar isotopic system in phlogopite and phengitic K-white mica, which is known to be ~400 °C and ~360 °C, respectively [39–41], the whole rock age for massive hornfels and phyllonites (~133 Ma and 126 Ma to 112 Ma, respectively) most likely reflect incomplete resetting of older radioisotopic systems during the mylonitic overprint. However, the detrital effect can be negligible in illite concentrates due to the lower closing temperature of fine-grained illite crystals (~260 °C; [40,41]). The K–Ar age of 98 Ma and 96 Ma for the separated clay fraction (<2 µm) together with the age of the K-feldspar crack fillings in the vein tourmaline and the phlogopite concentrates, is in good agreement with the  $^{40}\text{Ar}/^{39}\text{Ar}$  age of 100 Ma [17], which can date the shearing and accompanying metamorphism.

## 6. Conclusions

This study highlights the main metasomatic effects and paragenetic sequences of granite-related mineralizations in Highiş granitoids, Apuseni Mountains, Romania. The following conclusions can be drawn about the studied granitoid and country rocks:

- (1) Several characteristic features of albitization, sericitization, tourmalinization, epidotization, and hematitization were recognized in the studied samples. In the paragenetic sequence, three different hydrothermal episodes can be demonstrated: (i) crystallization of UST quartz, K-feldspar, and magnetite, representing the first stage during the magmatic-hydrothermal transition; (ii) the early and main stages of greisenization with a mineral assemblage of albite, 'sericite', schorl, and quartz; and (iii) the late vein-depositing stage with mineral assemblages of dravite, quartz, 'specularite', epidote, apatite and, subsequently, albite and mica.
- (2) Felsic rock samples contain at least two generations of tourmaline (group I tourmaline: schorl, group II tourmaline: dravite), supporting that these rocks were affected by multiple hydrothermal events. The country rocks also have disseminated tourmaline and tourmaline-quartz-dominated veins. Therefore, the study area could belong to a boron-rich open greisen system in the apical portion of the Highiş granite.
- (3) In the contact aureole, spotted schists with the presence of porphyroblastic biotite and cordierite occur. The observed mineralogical assemblages together with the petrographic features show that the thermal mineral assemblages were overprinted by greisenization. Furthermore, exogreisen deposits developed in both pelitic and mafic rocks in the study area.
- (4) Based on our results, the previously published Permian crystallization ages could be homogenized and/or partially rejuvenated during the hydrothermal mineralization processes. Additionally, the Highiş granite-related magmatic-hydrothermal system also suffered a Cretaceous thermal overprint.

**Author Contributions:** Conceptualization, A.V.; methodology, A.V., B.R., N.Z., B.T. and Z.B.; formal analysis, A.V., B.R., A.P., N.Z., B.T. and Z.B.; investigation, A.V., B.R., A.P., N.Z., B.T. and Z.B.; resources, A.V., B.R. and A.P.; writing—original draft preparation and editing, A.V.; writing—review, B.R., N.Z., Z.B., B.T. and E.P.-M.; visualization, A.V., B.R. and A.P.; supervision, A.V.; project administration, A.V. and B.R.; funding acquisition, A.V. and E.P.-M. All authors have read and agreed to the published version of the manuscript.

**Funding:** This research was financially supported by the National Research, Development, and Innovation Fund (grant numbers K 108375 and K 131690).

**Data Availability Statement:** All data supporting the reported results can be found in the manuscript and its appendices.

**Acknowledgments:** Sample preparation for petrographic investigation was made by Attila Bencsik and Viktor Granyák (University of Szeged). Thanks to the Department of Mineral Sciences, Smithsonian National Museum of Natural History, Washington, USA for providing some WDX standards.

**Conflicts of Interest:** The authors declare no conflict of interest. The funders had no role in the design of the study; in the collection, analyses, or interpretation of data; in the writing of the manuscript; or in the decision to publish the results.



## Appendix A

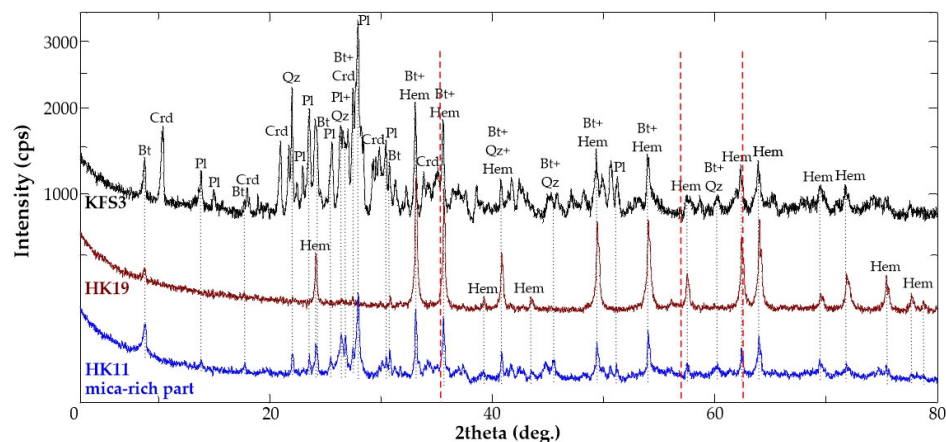


**Figure A1.** X-ray powder diffractograms of selected samples (for further information, see Table 1). The red dashed lines indicate the positions of the main reflections of magnetite (not detected) at 2.530 Å, 1.614 Å, and 1.483 Å, corresponding to the relative intensity value of 100, 85, and 85, respectively. Mineral abbreviations: Bt, biotite; Crd, cordierite; Hem, hematite; Pl, plagioclase; Qz, quartz.

## Appendix B

**Table A1.** Representative electron microprobe analyses of group I tourmaline in wt%. Two types of first-generation schorl tourmaline are distinguished based on their chemical composition. The chemical formulas of tourmaline were calculated based on 31 anions, corresponding to the general formula:  $XY_3Z_6T_6O_{18}(BO_3)_3V_3W$  [24,25].

Title	Tur I 1a	Tur I 1b	Tur I 1c	Tur I 1d	Tur I 1e	Tur I 1f	Tur I 2a	Tur I 2b
SiO <sub>2</sub>	35.1	35.08	34.82	35.68	35.78	35.56	34.54	34.57
TiO <sub>2</sub>	0.68	0.58	0.62	0.56	0.84	0.82	1.15	1.2
Al <sub>2</sub> O <sub>3</sub>	23.65	24.08	24.02	24.83	24.11	24.28	20.2	20.31
FeO *	12.68	12.97	12.37	12.44	12.06	12.14	15.36	15.75
MgO	8.89	8.63	9.23	8.64	9.3	9.2	8.97	8.91
CaO	1.92	1.6	1.96	1.51	2.05	1.89	2.63	2.76
MnO	0.09	0.05	0.05	0.06	0.05	0.06	0.12	0.1
Na <sub>2</sub> O	1.7	2.04	1.7	1.92	1.76	1.67	1.46	1.53
K <sub>2</sub> O	0	0.03	0	0.03	0.03	0	0.01	0.03
H <sub>2</sub> O **	3.44	3.45	3.45	3.50	3.51	3.50	3.36	3.37
B <sub>2</sub> O <sub>3</sub> ***	9.98	10.01	10.00	10.14	10.17	10.13	9.72	9.78
Li <sub>2</sub> O ****	0.00	0.00	0.00	0.00	0.00	0.00	0.00	0.00
Total	98.13	98.52	98.22	99.31	99.66	99.25	97.52	98.31
Structural formula based on 31 anions (O, OH, F)								
Si	6.11	6.09	6.05	6.12	6.12	6.10	6.17	6.14
Al	0.00	0.00	0.00	0.00	0.00	0.00	0.00	0.00
ΣT	6.11	6.09	6.05	6.12	6.12	6.10	6.17	6.14
B	3.00	3.00	3.00	3.00	3.00	3.00	3.00	3.00
ΣB	3.00	3.00	3.00	3.00	3.00	3.00	3.00	3.00
Al	4.86	4.93	4.92	5.02	4.86	4.91	4.26	4.25
Mg	1.15	1.07	1.08	0.98	1.14	1.09	1.75	1.75
ΣZ	6.00	6.00	6.00	6.00	6.00	6.00	6.00	6.00
Al	0.00	0.00	0.00	0.00	0.00	0.00	0.00	0.00
Ti	0.09	0.08	0.08	0.07	0.11	0.11	0.16	0.16
Mg	1.16	1.16	1.31	1.22	1.23	1.26	0.65	0.62
Mn	0.01	0.01	0.01	0.01	0.01	0.01	0.02	0.02
Fe <sup>2+</sup>	1.85	1.88	1.80	1.78	1.72	1.74	2.30	2.34
ΣY	3.11	3.13	3.20	3.09	3.06	3.12	3.11	3.13

Table A1. Cont.

Title	Tur I 1a	Tur I 1b	Tur I 1c	Tur I 1d	Tur I 1e	Tur I 1f	Tur I 2a	Tur I 2b
Ca	0.36	0.30	0.37	0.28	0.38	0.35	0.50	0.53
Na	0.57	0.69	0.57	0.64	0.58	0.56	0.51	0.53
K	0.00	0.01	0.00	0.01	0.01	0.00	0.00	0.01
$\Sigma X$	0.93	0.99	0.94	0.92	0.97	0.90	1.01	1.06
OH	4.00	4.00	4.00	4.00	4.00	4.00	4.00	4.00
$\Sigma V + W$	4.00	4.00	4.00	4.00	4.00	4.00	4.00	4.00
Mineral name	Schorl	Schorl	Schorl	Schorl	Schorl	Schorl	Schorl	Schorl

FeO \* Total iron was regarded as FeO. H<sub>2</sub>O \*\* H<sub>2</sub>O calculated from stoichiometry: OH + F = 4 apfu. B<sub>2</sub>O<sub>3</sub> \*\*\* B<sub>2</sub>O<sub>3</sub> calculated from stoichiometry: B = 3 apfu. Li<sub>2</sub>O \*\*\*\* Li<sub>2</sub>O calculated from stoichiometry: Li = 15 – total (T + Z + Y). The calculated compositions of the tourmaline types are the following: type 1: (Na<sub>0.60</sub>Ca<sub>0.34</sub>K<sub>0.01</sub>) $\Sigma$  = 0.94(Fe<sup>2+</sup><sub>1.80</sub>Mg<sub>1.22</sub>Ti<sub>0.09</sub>Mn<sub>0.01</sub>) $\Sigma$  = 3.12(Al<sub>4.92</sub>Mg<sub>1.08</sub>) $\Sigma$  = 6.00Si<sub>6</sub>O<sub>18</sub>(BO<sub>3</sub>)<sub>3</sub>(OH)<sub>4</sub>. type 2: (Na<sub>0.52</sub>Ca<sub>0.51</sub>K<sub>0.01</sub>) $\Sigma$  = 1.04(Fe<sup>2+</sup><sub>2.32</sub>Mg<sub>0.63</sub>Ti<sub>0.16</sub>Mn<sub>0.02</sub>) $\Sigma$  = 3.13(Al<sub>4.26</sub>Mg<sub>1.75</sub>) $\Sigma$  = 6.00Si<sub>6</sub>O<sub>18</sub>(BO<sub>3</sub>)<sub>3</sub>(OH)<sub>4</sub>.

**Table A2.** Representative electron microprobe analyses of group II tourmaline in wt%. The chemical formulas of tourmaline were calculated based on 31 anions, corresponding to the general formula: XY<sub>3</sub>Z<sub>6</sub>T<sub>6</sub>O<sub>18</sub>(BO<sub>3</sub>)<sub>3</sub>V<sub>3</sub>W [24,25].

Title	Tur II 3a <sup>1</sup>	Tur II 3b	Tur II 3c	Tur II 3d <sup>1</sup>	Tur II 3e	Tur II 3f	Tur II 3g <sup>1</sup>	Tur II 3h	Tur II 3i
SiO <sub>2</sub>	35.98	37.12	36.76	36.05	36.24	36.63	36.42	36.96	36.99
TiO <sub>2</sub>	0.37	0.06	0.08	0.4	0.12	0.12	0.45	0.07	0.13
Al <sub>2</sub> O <sub>3</sub>	27.76	32.19	32	28.64	31.13	31.25	29.5	32.05	32.15
FeO *	11.04	6.24	6.49	10.07	6.7	6.9	8.15	6.95	6.73
MgO	7.75	8.07	7.91	7.61	7.79	7.92	8.37	8.05	8.12
CaO	1.36	0.35	0.41	1.11	0.51	0.48	1.06	0.5	0.35
MnO	0.08	0.05	0.04	0	0.03	0	0.06	0.03	0.07
Na <sub>2</sub> O	2.1	2.44	2.54	2.18	2.39	2.47	2.31	2.41	2.42
K <sub>2</sub> O	0.01	0.04	0.02	0.03	0.02	0	0.02	0.03	0.01
H <sub>2</sub> O **	3.57	3.70	3.68	3.58	3.62	3.65	3.63	3.71	3.71
B <sub>2</sub> O <sub>3</sub> ***	10.35	10.73	10.67	10.39	10.49	10.58	10.53	10.74	10.75
Li <sub>2</sub> O ****	0.00	0.00	0.00	0.00	0.00	0.00	0.00	0.00	0.00
Total	100.38	101.00	100.60	100.06	99.03	100.00	100.50	101.50	101.43

Structural formula based on 31 anions (O, OH, F)

Si	6.04	6.01	5.99	6.03	6.01	6.02	6.01	5.98	5.98
Al	0.00	0.00	0.01	0.00	0.00	0.00	0.00	0.02	0.02
$\Sigma T$	6.04	6.01	6.00	6.03	6.01	6.02	6.01	6.00	6.00
B	3.00	3.00	3.00	3.00	3.00	3.00	3.00	3.00	3.00
$\Sigma B$	3.00	3.00	3.00	3.00	3.00	3.00	3.00	3.00	3.00
Al	5.49	6.00	6.00	5.65	6.00	6.00	5.74	6.00	6.00
Mg	0.51	0.00	0.00	0.35	0.00	0.00	0.26	0.00	0.00
$\Sigma Z$	6.00	6.00	6.00	6.00	6.00	6.00	6.00	6.00	6.00
Al	0.00	0.14	0.13	0.00	0.08	0.05	0.00	0.09	0.11
Ti	0.05	0.01	0.01	0.05	0.02	0.02	0.06	0.01	0.02
Mg	1.43	1.95	1.92	1.55	1.93	1.94	1.80	1.94	1.96
Mn	0.01	0.01	0.01	0.00	0.00	0.00	0.01	0.00	0.01
Fe <sup>2+</sup>	1.55	0.85	0.88	1.41	0.93	0.95	1.13	0.94	0.91
$\Sigma Y$	3.04	2.95	2.95	3.01	2.95	2.95	2.99	2.99	3.00
Ca	0.25	0.06	0.07	0.20	0.09	0.08	0.19	0.09	0.06
Na	0.68	0.77	0.80	0.71	0.77	0.79	0.74	0.76	0.76
K	0.00	0.01	0.00	0.01	0.00	0.00	0.00	0.01	0.00
$\Sigma X$	0.93	0.84	0.88	0.91	0.86	0.87	0.93	0.85	0.82
OH	4.00	4.00	4.00	4.00	4.00	4.00	4.00	4.00	4.00
$\Sigma V + W$	4.00	4.00	4.00	4.00	4.00	4.00	4.00	4.00	4.00
Mineral name	Schorl	Dravite	Dravite	Dravite	Dravite	Dravite	Dravite	Dravite	Dravite

<sup>1</sup> Transition from group I to group II. FeO \* Total iron was regarded as FeO. H<sub>2</sub>O \*\* H<sub>2</sub>O calculated from stoichiometry: OH + F = 4 apfu. B<sub>2</sub>O<sub>3</sub> \*\*\* B<sub>2</sub>O<sub>3</sub> calculated from stoichiometry: B = 3 apfu. Li<sub>2</sub>O \*\*\*\* Li<sub>2</sub>O calculated from stoichiometry: Li = 15 – total (T + Z + Y). The calculated composition of the tourmaline type 3 is the following: (Na<sub>0.78</sub>Ca<sub>0.08</sub>) $\Sigma$  = 0.86(Mg<sub>1.94</sub>Fe<sup>2+</sup><sub>0.91</sub>Al<sub>0.10</sub>Ti<sub>0.02</sub>Mn<sub>0.01</sub>) $\Sigma$  = 2.98Al<sub>6.00</sub>Si<sub>6</sub>O<sub>18</sub>(BO<sub>3</sub>)<sub>3</sub>(OH)<sub>4</sub>.

## References

- Štemprok, M. Greisenization (a review). *Geol. Rundsch.* **1987**, *76*, 169–175. [\[CrossRef\]](#)
- Pirajno, F. *Hydrothermal Processes and Mineral Systems*; Springer Science + Business Media B.V.: Berlin/Heidelberg, Germany, 2009; pp. 205–259. [\[CrossRef\]](#)
- Pirajno, F. Effects of Metasomatism on Mineral Systems and Their Host Rocks: Alkali Metasomatism, Skarns, Greisens, Tourmalinites, Rodingites, Black-Wall Alteration and Listvenites. In *Metasomatism and the Chemical Transformation of Rock*; Harlov, D.E., Austrheim, H., Eds.; Lecture Notes in Earth System Sciences; Springer: Berlin/Heidelberg, Germany, 2013; pp. 203–251. [\[CrossRef\]](#)
- Müller, A.; Herklotz, G.; Giegling, H. Chemistry of quartz related to the Zinnwald/Cínovec Sn-W-Li greisen-type deposit, Eastern Erzgebirge, Germany. *J. Geochem. Explor.* **2018**, *190*, 357–373. [\[CrossRef\]](#)
- Mohammadi, N.; McFarlane, C.R.M.; Lentz, D.R. U–Pb Geochronology of Hydrothermal Monazite from Uraniferous Greisen Veins Associated with the High Heat Production Mount Douglas Granite, New Brunswick, Canada. *Geosciences* **2019**, *9*, 224. [\[CrossRef\]](#)
- Chen, L.-L.; Ni, P.; Dai, B.-Z.; Li, W.-S.; Chi, Z.; Pan, J.-Y. The Genetic Association between Quartz Vein- and Greisen-Type Mineralization at the Maoping W–Sn Deposit, Southern Jiangxi, China: Insights from Zircon and Cassiterite U–Pb Ages and Cassiterite Trace Element Composition. *Minerals* **2019**, *9*, 411. [\[CrossRef\]](#)
- Radvanec, M.; Gonda, S. Genetic model of Permian hydrothermal mineralization in Gemeric unit (W. Carpathians) from the deep-seated zone of anatectic melting to volcanic-exhalative SedEx mineralization on the surface. *Miner. Slov.* **2019**, *52*, 109–156.
- Tillberg, M.; Maskenskaya, O.M.; Drake, H.; Hogmalm, J.K.; Broman, C.; Fallick, A.E.; Åström, M.E. Fractionation of Rare Earth Elements in Greisen and Hydrothermal Veins Related to A-Type Magmatism. *Geofluids* **2019**, *2019*, 4523214. [\[CrossRef\]](#)
- Stoltznow, M.; Lüders, V.; de Graaf, S.; Niedermann, S. A geochemical study of the Sweet Home mine, Colorado Mineral Belt, USA: Formation of deep hydrothermal vein-type molybdenum greisen and base metal mineralization. *Miner. Depos.* **2022**, *57*, 801–825. [\[CrossRef\]](#)
- Bonin, B.; Tatu, M. Cl-rich hydrous mafic mineral assemblages in the Highiş massif, Apuseni Mountains, Romania. *Miner. Petrol.* **2016**, *110*, 447–469. [\[CrossRef\]](#)
- Szemerédi, M.; Varga, A.; Dunkl, I.; Lukács, R.; Seghedi, I.; Kovács, Z.; Raucsik, B.; Pál–Molnár, E. Petrology and zircon U–Pb dating of granitoid rocks in the Highiş massif (SW Apuseni Mts., Romania): Insights into Permian plutonic–volcanic connections. *Geol. Carpath.* **2021**, *72*, 482–504. [\[CrossRef\]](#)
- Ciobanu, C.L.; Cook, N.J.; Damian, F.; Damian, G. Gold scavenged by bismuth melts: An example from Alpine shear-remobilizes in the Highiş Massif, Romania. *Miner. Petrol.* **2006**, *87*, 351–384. [\[CrossRef\]](#)
- Bordea, S.; Bordea, J. Presence of the “Vermiculate Sandstone Formation” (Permian) in the central zone of the Highiş mountains. *Rom. J. Stratigr.* **1993**, *75*, 17–19.
- Bejenaru, C.; Cioloboc, D. Uranium exploration and production in Romania: Case histories and prospects. In *Recent Developments in Uranium Resources and Supply*; IAEA-TECDOC-823; International Atomic Energy Agency (IAEA): Vienna, Austria, 1995.
- Word Distribution of Uranium Deposits (UDEPO) with Uranium Deposit Classification; IAEA-TECDOC-1629; International Atomic Energy Agency (IAEA): Vienna, Austria. 2009. Available online: [https://www-pub.iaea.org/mtcd/publications/pdf/te\\_1629\\_web.pdf](https://www-pub.iaea.org/mtcd/publications/pdf/te_1629_web.pdf) (accessed on 21 May 2023).
- Kounov, A.; Schmid, S.M. Fission-track constraints on the thermal and tectonic evolution of the Apuseni Mountains (Romania). *Int. J. Earth Sci.* **2013**, *102*, 207–233. [\[CrossRef\]](#)
- Dallmeyer, R.D.; Pană, D.I.; Neubauer, F.; Erdmer, P. Tectonothermal evolution of the Apuseni Mountains, Romania; resolution of Variscan versus Alpine events with  $^{40}\text{Ar}/^{39}\text{Ar}$  ages. *J. Geol.* **1999**, *107*, 329–352. [\[CrossRef\]](#)
- Balintoni, I.; Balica, C.; Cliveți, M.; Li, L.Q.; Hann, H.P.; Chen, F.; Schuller, V. The emplacement age of the Muntele Mare Variscan granite (Apuseni Mountains, Romania). *Geol. Carpath.* **2009**, *60*, 495–504. [\[CrossRef\]](#)
- Papiu, C.V.; Ghenea, C. *Geological Map of Romania, Arad Sheet 16, Scale: 1:200,000*; Geological Institute of Romania: Bucharest, Romania, 1966.
- Pană, D.I.; Heaman, L.M.; Creaser, R.A.; Erdmer, P. Pre-Alpine crust in the Apuseni Mountains, Romania: Insights from Sm–Nd and U–Pb data. *J. Geol.* **2002**, *110*, 341–354. [\[CrossRef\]](#)
- Pană, D.I.; Ricman, C. The lower complex of the Paiușeni series—A blastomylonitic shear belt. *Rev. Roum. Géol. Géophys. Géogr. Géologie* **1988**, *32*, 21–35.
- Pană, D.I.; Erdmer, P. Alpine crustal shear zones and pre-alpine basement terranes in the Romanian Carpathians and Apuseni Mountains. *Geology* **1994**, *22*, 807–810. [\[CrossRef\]](#)
- Whitney, D.L.; Evans, B.W. Abbreviations for names of rock-forming minerals. *Am. Min.* **2010**, *95*, 185–187. [\[CrossRef\]](#)
- Pouchou, J.-L.; Pichoir, F. A new model for quantitative X-ray micro-analysis. *Rech. Aerosp.* **1984**, *3*, 167–192.
- Selway, J.B.; Xiong, J. Tourmaline recalculation software (Excel spreadsheet: Tourmaline.xls). Tindle, A.G.; Breaks, F.W.; Selway, J.B. Tourmaline in petalite-subtype granitic pegmatites: Evidence of fractionation and contamination from the Pakeagama Lake and Separation Lake areas of northwestern Ontario, Canada. *Can. Miner.* **2002**, *40*, 753–788. [\[CrossRef\]](#)
- Henry, D.J.; Novák, M.; Hawthorne, F.C.; Ertl, A.; Dutrow, B.L.; Uher, P.; Pezzotta, F. Nomenclature of the tourmaline-super group minerals. *Am. Min.* **2011**, *96*, 895–913. [\[CrossRef\]](#)
- Matsumoto, A.; Kobayashi, T. K–Ar age determination of late Quaternary volcanic rocks using the “mass fractionation correction procedure”: Application to the Younger Ontake Volcano, central Japan. *Chem. Geol.* **1995**, *125*, 123–135. [\[CrossRef\]](#)



28. Ottens, B.; Schuster, R.; Benkó, Z. The Secondary Minerals from the Pillow Basalt of Salsette-Mumbai, Deccan Volcanic Province, India. *Minerals* **2022**, *12*, 444. [\[CrossRef\]](#)
29. Hess, J.C.; Lippolt, H.J. Compilation of K-Ar measurements on HDB-1 standard biotite. Status Report. In *Phanerozoic Time Scale, Bulletin de Liaison et D'information*; IUGS Subcommission on Geochronology: Paris, France, 1994; pp. 19–23.
30. Gillot, P.-Y.; Cornette, Y.; Max, N.; Floris, B. Two Reference Materials, Trachytes Mdo-G and Ish-G, for Argon Dating (K-Ar and  $^{40}\text{Ar}/^{39}\text{Ar}$ ) of Pleistocene and Holocene Rocks. *Geostand. Newsl.* **1992**, *16*, 55–60. [\[CrossRef\]](#)
31. Steiger, R.; Jäger, E. Subcommission on geochronology: Convention on the use of decay constants in geo and cosmochronology. *Earth Planet. Sci. Lett.* **1977**, *36*, 359–362. [\[CrossRef\]](#)
32. Quidelleur, X.; Gillot, P.-Y.; Soler, V.; Lefèvre, J.C. K/Ar dating extended into the last millennium: Application to the youngest effusive episode of the Teide volcano (Spain). *Geophys. Res. Lett.* **2001**, *28*, 3067–3070. [\[CrossRef\]](#)
33. Hanesch, M. Raman spectroscopy of iron oxides and (oxy)hydroxides at low laser power and possible applications in environmental magnetic studies. *Geophys. J. Int.* **2009**, *177*, 941–948. [\[CrossRef\]](#)
34. Müller, A.; Kirwin, D.; Seltmann, R. Textural characterization of unidirectional solidification textures related to Cu–Au deposits and their implication for metallogenesis and exploration. *Miner. Depos.* **2023**. [\[CrossRef\]](#)
35. Zharikov, V.A.; Rusinov, V.L.; Marakushev, A.A.; Zharaisky, G.P.; Omelianenko, B.I.; Pertsev, N.N.; Rass, I.T.; Andreeva, O.V.; Abramov, S.S.; Podlessky, K.V.; et al. Metasomatism and Metasomatic Rocks, English Translation. 2015. Available online: [https://archive.org/details/metasomatic\\_rocks\\_april\\_2015/mode/2up](https://archive.org/details/metasomatic_rocks_april_2015/mode/2up) (accessed on 30 December 2022).
36. Kubiš, M.; Broska, I. The role of boron and fluorine in evolved granitic rock systems (on the example of the Hnilec area, Western Carpathians). *Geol. Carpath.* **2005**, *56*, 193–204. Available online: <http://www.geologicacarthica.com/browse-journal/volumes/56-3/article-309/> (accessed on 21 May 2023).
37. de Oliveira, L.A.R.; Rios, F.J.; Rosière, C.A.; Wälle, M.; Ortelli, M.; Kouzmanov, K. Nature and evolution of fluids associated with specularite-bearing Fe and Au-PGE (Jacutinga) mineralization during the Brasiliano orogeny in the eastern São Francisco Craton, Minas Gerais, Brazil. *Ore Geol. Rev.* **2017**, *86*, 130–153. [\[CrossRef\]](#)
38. Liu, X.; Zhang, D.; Yang, J.; Xiao, C.; Zhang, T. High heat producing granites and prolonged extraction of tungsten and tin from melts. *Geochim. Cosmochim. Acta* **2023**, *348*, 340–354. [\[CrossRef\]](#)
39. Hodges, K.V. Geochronology and Thermochronology in Orogenic Systems. In *Treatise on Geochemistry*; Rudnick, R.L., Holland, H.D., Turekian, K.K., Eds.; Elsevier: Oxford, UK, 2003; Volume 3, pp. 263–292. [\[CrossRef\]](#)
40. Hunziker, J.C. The evolution of illite to muscovite: An example of the behaviour of isotopes in low-grade metamorphic terrains. *Chem. Geol.* **1986**, *57*, 31–40. [\[CrossRef\]](#)
41. Hunziker, J.C.; Frey, M.; Clauer, N.; Dallmeyer, R.D.; Friedrichsen, H.; Flehmig, W.; Hochstrasser, K.; Roggwiler, P.; Schwander, H. The evolution of illite to muscovite: Mineralogical and isotopic data from the Glarus Alps, Switzerland. *Contrib. Miner. Petrol.* **1986**, *92*, 157–180. [\[CrossRef\]](#)

**Disclaimer/Publisher's Note:** The statements, opinions and data contained in all publications are solely those of the individual author(s) and contributor(s) and not of MDPI and/or the editor(s). MDPI and/or the editor(s) disclaim responsibility for any injury to people or property resulting from any ideas, methods, instructions or products referred to in the content.